

Single- and two-particle observables in the Emery model: a dynamical mean-field perspective

Yi-Ting Tseng¹, Mario O. Malcolms², Henri Menke¹, Marcel Klett²,
Thomas Schäfer², Philipp Hansmann^{1*}

1 Department of Physics, Friedrich-Alexander-Universität Erlangen-Nürnberg, 91058
Erlangen, Germany

2 Max Planck Institute for Solid State Research, Heisenbergstraße 1, 70569 Stuttgart,
Germany

*philipp.hansmann@fau.de

September 11, 2024

Abstract

We investigate dynamical mean-field calculations of the three-band Emery model at the one- and two-particle level for material-realistic parameters of high- T_c superconductors. Our study shows that even within dynamical mean-field theory, which accounts solely for temporal fluctuations, the intrinsic multi-orbital nature of the Emery model introduces effective non-local correlations. These correlations lead to a non-Curie-like temperature dependence of the magnetic susceptibility, consistent with nuclear magnetic resonance experiments in the pseudogap regime. By analyzing the temperature dependence of the static dynamical mean-field theory spin susceptibility, we find indications of emerging oxygen-copper singlet fluctuations, explicitly captured by the model. Despite correctly describing the hallmark of the pseudogap at the two-particle level, such as the drop in the Knight shift of nuclear magnetic resonance, dynamical mean-field theory fails to capture the spectral properties of the pseudogap.

1 Introduction

Predictive calculations for emergent phenomena in correlated condensed matter systems are a contemporary focus of a large research community. One of the principal and notorious paradigms in this field is the unconventional superconductivity in hole- and electron-doped cuprates [1, 2]. The ionic electronic configuration of copper in these compounds suggests a single half-filled band of $d_{x^2-y^2}$ character which is usually modeled by the famous single-band Hubbard model [3–6]. Alternative models that include also oxygen $2p$ -orbitals were proposed by Emery [7] and refined by Andersen [8]. While the single band model is, due to its simplicity, very attractive for the treatment even with demanding quantum many-body methods [9, 10], the appeal of the Emery model is the explicit inclusion of higher energy excitations such as charge-transfer processes.

To reach superconductivity, cuprates must be doped at sufficiently low temperatures [11, 12]. Therefore, the accuracy of a calculation for cuprates is primarily evaluated by comparison to experiments in the temperature-versus-doping phase diagram. From the theoretical perspective, the ideal calculation should allow for predictions of all trends in this phase diagram instead of capturing single points with adjusted parameters. At zero doping, the antiferromagnetic insulating character of the ground state of the parent

compounds can be reproduced even by a static mean-field calculation. At higher temperatures, the paramagnetic insulating state is captured by dynamical mean-field theory (DMFT) [13–15] as a Mott insulator. On the other side of the doping axis, at extremely high hole concentrations, the system behaves like a normal Fermi liquid, which can also be captured by DMFT. The challenge lies in connecting these extremes and capturing the famous pseudogap phase [16–18], as well as the superconducting dome below a strange metallic phase that does not behave like a Fermi liquid (e.g., optical conductivity [19]) and has a non-Curie-like magnetic response [11]. Nuclear magnetic resonance (NMR) has proven to be an indispensable experimental tool for analyzing magnetic properties in these regimes [16, 20–22], specifically for the onset of the pseudogap, which is signaled by a drop in the NMR Knight shift.

The strength of DMFT is its ability to cross non-perturbatively from the weak to the strong coupling limit. Yet, due to the local nature (i.e., no momentum dependence of correlations) of the DMFT approximation its application to the two-dimensional single-band Hubbard model fails dramatically when compared to experiments at low temperatures. Curing this deficiency of DMFT towards the inclusion of non-local correlations became the motor for the development of a plethora of cluster-based or diagrammatic extensions of DMFT [23, 24]. Instead, when DMFT is applied to the three-band model in the localized Wannier orbital basis, its self-energy in the basis of the quasiparticle bands becomes momentum-dependent due to the mixed orbital nature of the Bloch bands. Such effective non-locality within the DMFT framework is known and has been pointed out, e.g. in multi-orbital models for nickelates [25, 26], and ruthenates [27, 28]. While much fewer in number compared to the single-band case, there have been some studies of the Emery model with DMFT showing good agreement with experiments at the one-particle level [29–32].

In the present work, we focus on the application of single-site DMFT to the Emery model, emphasizing doping and temperature dependencies at the single- and two-particle levels. Our results include single-particle spectra and static spin susceptibilities as a function of temperature and doping. We find good agreement of our calculations with nuclear magnetic resonance (NMR) experiments of Sr-doped $\text{La}_{2-x}\text{Sr}_x\text{CuO}_4$ [21, 33].

2 Models and Method

In the present study, we analyze the three-band Emery model within DMFT using material-realistic ab-initio model parameters (hopping and interaction) derived in [34, 35]. Specifically, the three-band model consists of one planar Cu $d_{x^2-y^2}$ and two oxygen (p_x and p_y) basis orbitals in the unit cell. While the original formulation [7] included only one d - p hopping integral in addition to the Hubbard interaction on the $d_{x^2-y^2}$ orbital, later works, particularly by Andersen et al. [8], refined the parameters to be closer to a material-realistic regime, including intra-oxygen t_{pp} terms. For our model, we use the tight-binding parameters derived from downfolded DFT (LAPW) calculations by Weber et al. [34] and we adopt the same convention as Kowalski et al. [35], with $\varepsilon_d = 0.0$, $\varepsilon_p = 2.3$, $t_{pd} = 2.1$, $t'_{pp} = 0.2$, in the units of $t_{pp} = 0.65$ eV, including double-counting corrections. The resulting Hamiltonian reads

$$H_{dp}(\mathbf{k}) = H_0^{dp}(\mathbf{k}) + H_{int.}^{dp}(\mathbf{k}), \quad (1)$$

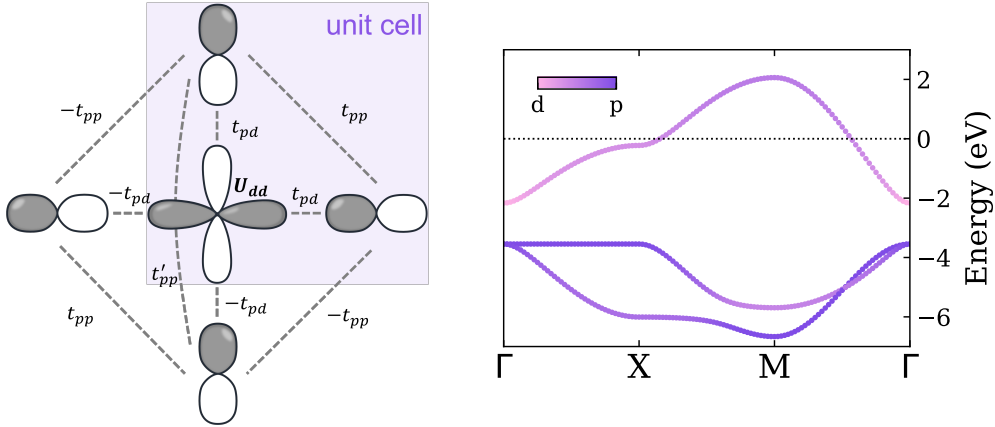


Figure 1: Left-hand side: Unit cell, hopping-, and interaction parameters in the Emery model. Right-hand side: Band structure with color coded orbital character.

where $H_0^{dp}(\mathbf{k})$ is the single-particle hopping part

$$H_0^{dp}(\mathbf{k}) = \begin{pmatrix} \varepsilon_d & t_{pd}(1 - e^{-ik_x}) & t_{pd}(1 - e^{-ik_y}) \\ t_{pd}(1 - e^{ik_x}) & \varepsilon_p + 2t'_{pp} \cos k_x & t_{pp}(1 - e^{ik_x})(1 - e^{-ik_y}) \\ t_{pd}(1 - e^{ik_y}) & t_{pp}(1 - e^{-ik_x})(1 - e^{ik_y}) & \varepsilon_p + 2t'_{pp} \cos k_y \end{pmatrix}. \quad (2)$$

Here ε_d and ε_p are the on-site energies of d - and p - orbitals. t_{pd} is nearest-neighbor hopping between Cu and O, t_{pp} (t'_{pp}) is (second) nearest-neighbor hopping between O and O as shown in schematic Fig. 1. For the interaction in Eq. (1) we follow [35] and include only U_{dd} as a local Hubbard repulsion

$$H_{int}^{dp}(\mathbf{k}) = U_{dd} \hat{n}_{d\uparrow} \hat{n}_{d\downarrow} \quad (3)$$

where $n_{d\sigma}$ is the density operator of quasiparticles in the Cu- d orbital with spin σ .

Single-site DMFT solver. To solve the model, we perform single-site DMFT calculations using continuous-time quantum Monte Carlo impurity solvers [36] in the hybridization expansion (CT-HYB). We use the w2dynamics code [37] and consider the $d_{x^2-y^2}$ orbital as the impurity in our dp -model with a local Hubbard term of $U_{dd} = 14 t_{pp} = 9.1$ eV. To obtain the single-particle spectrum, we converge the auxiliary Anderson model with a paramagnetic constraint.

Analytic continuation of the self-energy. To obtain the real-frequency self-energy, we perform a maximum entropy (MaxEnt) analytic continuation on an auxiliary Green function

$$G^{\text{aux}}(i\omega_n) = (i\omega_n + \mu^{\text{aux}} - \Sigma_{dd}(i\omega_n))^{-1} \quad (4)$$

with the Ω MaxEnt code [38] and subsequent inversion of the equation

$$\Sigma_{dd}(\omega) = \omega + \mu^{\text{aux}} - G^{\text{aux}}(\omega)^{-1}, \quad (5)$$

which we can use to compute the retarded lattice Green function

$$G_{\text{lat}}(\omega, \mathbf{k}) = ((\omega + \mu + i\delta)\mathbf{1} - H_0^{dp}(\mathbf{k}) - \Sigma^{\text{DMFT}}(\omega))^{-1} \quad (6)$$

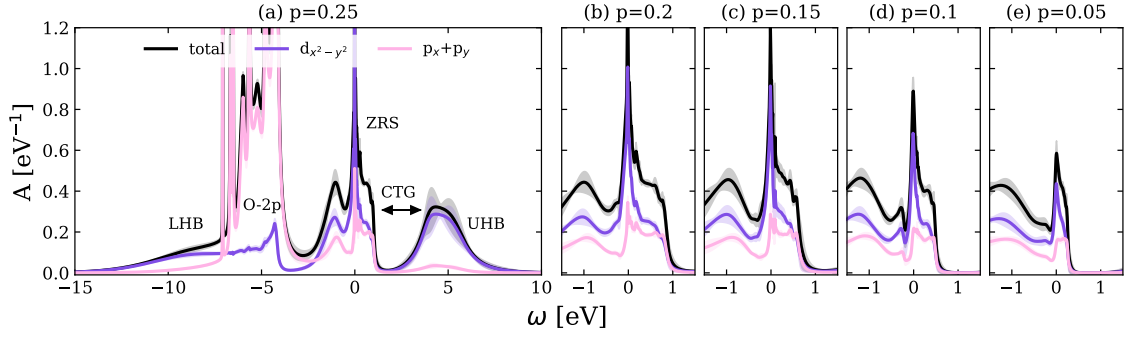


Figure 2: Doping- and orbital-dependent local spectral function $A_\alpha(\omega) = -\frac{1}{\pi} \sum_{\mathbf{k}} \text{Im}[G_{\text{lat}}(\omega, \mathbf{k})]_{\alpha, \alpha}$ for $U_{dd} = 9.1 \text{ eV}$ and $T \approx 150 \text{ K}$. The (light) black, purple, and pink line shows spectral function (error bar) contributed by total, $d_{x^2-y^2}$ and $p_x + p_y$ orbitals. The main features are indicated by labels and include the lower (LHB) and upper (LHU) Hubbard bands, p -bands which define a charge transfer gap (CTG), and a low energy Zhang-Rice singlet (ZRS) quasi-particle peak at the Fermi energy.

where the self-energy $\Sigma^{\text{DMFT}}(\omega) = \text{diag}(\Sigma_{dd}(\omega), 0, 0)$ is a diagonal 3×3 matrix with only one finite element, i.e. $\Sigma_{dd}(\omega)$ in the d -subspace. As the exact result of the self-energy is independent of μ^{aux} in Eq. 4, we used variations of this parameter to estimate the stability of the analytical continuation by means of error bars for the spectral function (gray shaded areas in Figs. 2 and 3).

Uniform magnetic susceptibility In order to extract the uniform/ferromagnetic, i.e. $\mathbf{q} = \mathbf{0}$, spin susceptibility, we measure the magnetization, $m = n_{d\uparrow} - n_{d\downarrow}$, in the presence of a small ferromagnetic field within the linear response regime, with field strength $H_{\text{ferro}} \approx 5 \text{ meV}$, and we obtain the slope of a linear fit which enables us to compute the uniform susceptibility as

$$\text{Re } \chi_m(i\Omega_0 = 0, \mathbf{q} = \mathbf{0}) = \left. \frac{\partial m}{\partial H} \right|_{H=0}. \quad (7)$$

3 Results

3.1 Single-particle spectra

In Fig. 2 we show the \mathbf{k} -integrated orbitally resolved spectral function for the Emery model defined in Eq. (1):

$$A_\alpha(\omega) = -\frac{1}{\pi} \sum_{\mathbf{k}} \text{Im}[G_{\text{lat}}(\omega, \mathbf{k})]_{\alpha, \alpha}, \quad (8)$$

where α is the orbital index. The computations have been performed for $U_{dd} = 9.1 \text{ eV}$ and at the temperature of $T \approx 150 \text{ K}$. In the panels from left to right we show results for different doping levels ranging from $p = 0.25$ to $p = 0.05$, where the doping level is defined as $p \equiv 5.0 - N$ (i.e. $p = 0.0$ corresponds to “half-filling”). In the plots we resolve the spectra into copper d - (dark violet) and oxygen p - (pink) orbital characters respectively. The shaded areas around the lines correspond to an error estimate (see Sec. 2 for details).

In the leftmost panel we show the spectra for the $p = 0.25$ case in a wide energy range from -15 eV to $+10$ eV and label the most significant spectral features. At larger energies we see clear Hubbard bands of copper- d character which are centered around -10 eV and $+5$ eV. In the area between -3 eV and -8 eV most of the oxygen- p spectral weight is found which in large parts is unaffected by correlation effects and identical to the DFT single-particle density of states (DOS) of oxygen (note that as we perform analytical continuation on the level of the self-energy which is finite only for the Cu d -orbital, the oxygen peaks are not subject to life time- and/or spurious MaxEnt broadening and remain maximally sharp). The most intriguing feature, however, is the sharp and pronounced quasiparticle peak at the Fermi level $\omega = 0$ of strongly mixed copper- d and oxygen- p character. If we follow this feature towards the half-filled limit ($p = 0.0$) we observe the expected sharpening and decrease in spectral weight which eventually will result in the metal-to-insulator transition and the opening of a gap at $p = 0.0$. The mixed copper-oxygen nature of this quasiparticle has been attributed to the formation of a Zhang-Rice singlet already in previous works [29–32, 35, 39]. We note that the charge-transfer gap (CTG) of our Emery-spectra is roughly between $1.5 - 2$ eV for lower doping and increases for larger values of p . This energy scale (and indeed the doping trend) is in agreement with experiments on the optical conductivity for Sr doped La_2CuO_4 [40].

Next, we analyze the analytically continued DMFT self-energy in the orbital basis and plot it in panel (a) of Fig. 3 covering the same doping levels as for the spectra. Also here the shaded areas indicate error bars estimated for the analytical continuation. At the highest doping levels the self-energy shows pronounced Fermi liquid behaviour for $T \approx 150$ K with a linear real part (from which the correlation induced mass-renormalization can be estimated) and an imaginary part $\propto \omega^2$. Closer to half-filling the real-part remains linear, but the quasiparticle scattering rate (i.e. $-\text{Im}\Sigma(\omega = 0)$) increases significantly with decreased hole-doping at constant temperature. Unsurprisingly, the \mathbf{k} -independent DMFT self-energy fails to capture the \mathbf{k} -selective pseudogap physics at small doping values. As we mentioned above, a projection on the quasiparticle band around ε_F would result in an effective \mathbf{k} -dependence of the self-energy for the low-energy quasiparticles as it would also implicitly encode information about the \mathbf{k} -dependent composition of the quasiparticles in terms of copper- d and oxygen- p character [25–28]. While such projection results in a \mathbf{k} -dependent mass renormalization, it would not change the overall Fermi-liquid behaviour and therefore cannot cure the DMFT shortcomings in capturing pseudogap physics, i.e., the gapped behaviour of the single-particle spectrum in the anti-nodal region.

We can, however, investigate whether the dependence of \mathbf{k}_F on the $k_{Fx} = k_{Fy}$ diagonal, is captured correctly by our calculations. To check this we plot the position of the quasiparticle pole on that diagonal for different dopings in panel (b) of Fig. 3 [same color coding as in panels (a)] and compare it to the experimental data shown in grey. As we can see the position of the nodal quasiparticle \mathbf{k}_F in the Brillouin zone is captured well by the DMFT spectral function for the Emery model: in our calculations as well as in the experiment for increased hole doping the nodal point is dragged towards the Γ -point of the Brillouin zone. For comparison we provide the result for the corresponding single-band calculation in the appendix App. A.

3.2 Magnetic susceptibility

We now turn to the results for the static uniform magnetic susceptibility. Fig. 4 (left) shows $\chi_{dd}(q = 0, \omega = 0) = \partial m / \partial H|_{H=0}$ which we obtained by converging the DMFT self-consistency cycle in the presence of a sufficiently small but finite uniform field $H \approx 5$ meV and subsequent measurements of the magnetization $m = n_{d\uparrow} - n_{d\downarrow}$. Our data covers temperatures from 250 K down to 30 K and the same doping ranges ($p = 0.05$ to 0.24) as

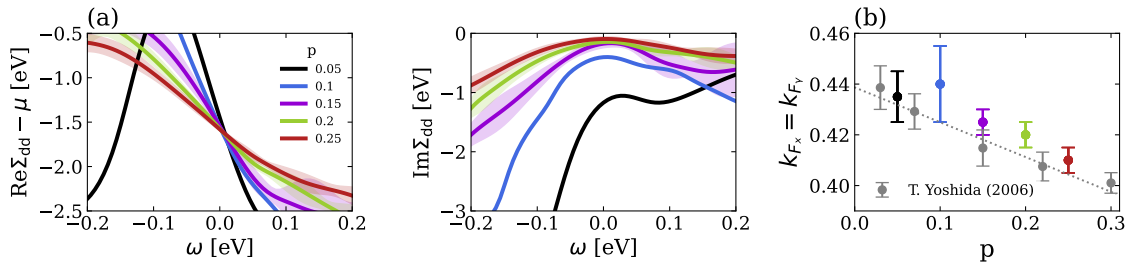


Figure 3: (a) Doping-dependent real-frequency self-energy (real and imaginary parts) of the d -orbital from analytic continuation. It shows Fermi-liquid behavior in a small ω region. (b) Doping dependence of the k_F value in the nodal direction. The calculation has been performed at $T \approx 150$ K. Experimental data are adapted from angle-resolved photoemission spectroscopy (ARPES) [41].

for the single-particle spectrum.

Overall, we observe a monotonous increase of $\chi_{dd}(\mathbf{q} = 0, \Omega = 0)$ upon hole-doping when keeping the temperature fixed. Further, for fixed doping, the temperature dependence has non-Curie-like behavior for all considered doping levels and shows a maximum that moves from $T_{\max} \approx 130$ K for the lowest doping to $T_{\max} \approx 100$ K at maximum doping. The observed behavior seems to be in line with experimental measurements of the NMR Knight shift for cuprates [21, 33, 42–44]. For a more quantitative comparison, we show a Clogston-Jaccarino plot in comparison to LSCO data in the right panel of Fig. 4. The points in this scatter plot have the experimentally observed Knight shift for $\text{La}_{2-x}\text{Sr}_x\text{CuO}_4$ for given temperature and doping as x -coordinate and the DMFT calculated χ_{dd} for the same parameters as y -coordinate. The plot suggests a linear relation between the two quantities and, hence, an excellent agreement of the temperature and doping trends in χ_{dd} captured by the calculation with the NMR measurement. In App. B we show that the occurrence of the temperature maximum of χ_{dd} in DMFT could be indicative of the emergence of copper-oxygen (Zhang-Rice) singlet fluctuations. As for the single particle spectrum, we provide the corresponding results for the single-band model in the appendix A.

At a first glance, it seems odd that DMFT for the Emery model reproduces the two-particle observable χ_{dd} better than the single-particle spectrum, for which it fails to capture the correct pseudogap behavior of the single-particle spectral function at lower doping levels. On the one hand it might be that the static *uniform* magnetic susceptibility measured by the NMR Knight shift is simply not too sensitive with respect to non-local correlations which are responsible for momentum-selective gapping of the Fermi surface. On the other hand there might be a methodological reason as well: In single-site DMFT, the correlations which are responsible for the downturn of χ_{dd} at lower temperatures give no feedback to the single-particle level. In order to test if a feedback of the two-particle level improves the single-particle spectra of the Emery model, calculations with methods incorporating these non-local correlations in the single-particle quantities [e.g., the dynamical vertex approximation (DVA), [24, 45]] will be carried out in a follow-up study.

4 Conclusions

In summary we have revisited a material realistic Emery model for cuprate high- T_c superconductors. We analyzed the model within the single-site DMFT framework and computed

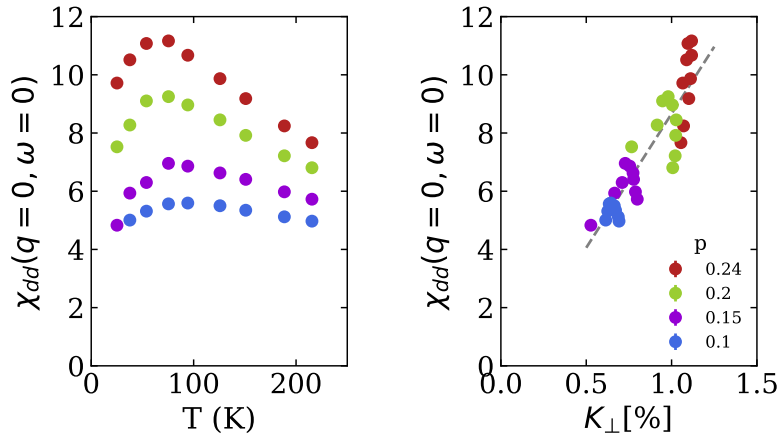


Figure 4: (left) dp-model spin susceptibility on d-orbital with doping $p=0.1-0.24$. (right) Clogston–Jaccarino plot: spin susceptibility of DMFT calculation (y-axis) is proportional to experimental NMR shift data (x-axis) from [21, 33].

observables corresponding to the single-particle spectral function accessible in (AR)PES experiments, as well as the two-particle correlation function of the magnetic susceptibility related to the NMR Knight shift. Comparison to experiments of both observables revealed that their doping and temperature dependencies can be captured well in the Emery picture for both single- and two-particle quantities within *one single set of model parameters*. This observation in combination with benchmarks of the single-band model (especially for the magnetic susceptibility; see App. A) for fixed parameters suggests that DMFT performs significantly better in predicting experimental observables for cuprates, and likely other charge transfer systems, when the oxygen degrees of freedom are included explicitly. This is in stark contrast, e.g., to infinite-layer nickelates, where theoretical single-band calculations agree well with doping trends seen in experiments [45–48]. However, there is no doubt about the failure of single-site DMFT for low dimensional systems at low temperatures and \mathbf{k} -selective gaps in the spectral function of the pseudogap regime remain surely beyond the grasp of an on-site self-energy even in the Emery model.

In follow-up studies we will continue our study for the Emery model beyond the single-site DMFT approximation. The inclusion of non-local correlations, e.g., with DGA, on the two-particle level will allow for a description of single- and two-particle level on equal footing within the pseudogap regime of cuprate compounds.

Acknowledgements

We thank Karsten Held, Matthias Hepting, Marc-Henri Julien, Giorgio Sangiovanni, Eric Jacob and Jörg Schmalian for helpful discussions. We acknowledge financial support by the DFG project HA7277/3-1. We thank the computing service facility of the MPI-FKF for their support and gratefully acknowledge the HPC resources (TinyFAT) administered by the RRZE of the Friedrich-Alexander-Universität Erlangen-Nürnberg (FAU).

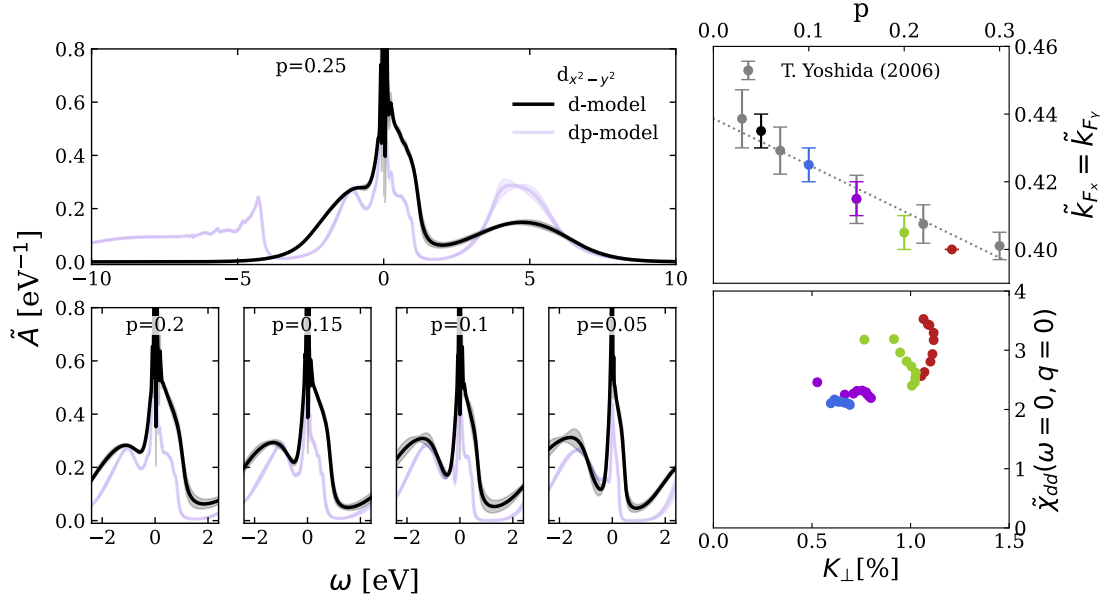


Figure 5: Single band model benchmarks. (a): Doping- and orbital-dependent local spectral function $\tilde{A}_\alpha(\omega) = -\frac{1}{\pi} \sum_{\mathbf{k}} \text{Im}[G_{\text{lat}}(\omega, \mathbf{k})]_{\alpha, \alpha}$ with $G_{\text{lat}}(\omega, \mathbf{k}) = ((\omega + \mu + i\delta)\mathbf{1} - H_0^d(\mathbf{k}) - \tilde{\Sigma}^{\text{DMFT}}(\omega))^{-1}$ at $\tilde{U}_{dd} = 5 \text{ eV}$, $T \approx 150 \text{ K}$. The (light) purple line shows the spectral function (error bar) of $d_{x^2-y^2}$. A quasiparticle peak is observed with all doping levels. (b): k_F of the nodal point compared to experiment. (c): d -model spin susceptibility vs. Knight shift.

A The single-band model

Single-band model benchmarks The downfolding step from the three- [Eq. (1)] to the single-band model is trivial as a simple diagonalization of the hopping matrix in momentum space automatically projects out the well-separated band at the Fermi level:

$$H_0^d(k) = 2\tilde{t}_{dd}(\cos k_x + \cos k_y) + 4\tilde{t}'_{dd} \cos k_x \cos k_y + \dots \quad (9)$$

For our calculations, we use the numerically evaluated Hamiltonian directly in momentum space. The corresponding hopping parameters are $\tilde{t}_{dd} = -0.51 \text{ eV}$ for the nearest- and $\tilde{t}'_{dd} = 0.026 \text{ eV}$ for the next-nearest neighbor terms. The interaction \tilde{U}_{dd} for the benchmark d -model calculations was adjusted by fitting the self-energy induced mass renormalization to the results of the dp -model. This estimate yielded $\tilde{U}_{dd} = 5 \text{ eV}$ for the corresponding single-band model.

Single-particle properties of dp -model can be well captured by the d -model as shown in Fig. 5 (a) and (b). The d -model shows Fermi-liquid-like self-energy and can reproduce the mass renormalization and k_F at the nodal point with $\tilde{U}_{dd} = 5 \text{ eV}$. However, it fails on two-particle properties as Clogston–Jaccarino plot diverges [Fig. 5 (c)].

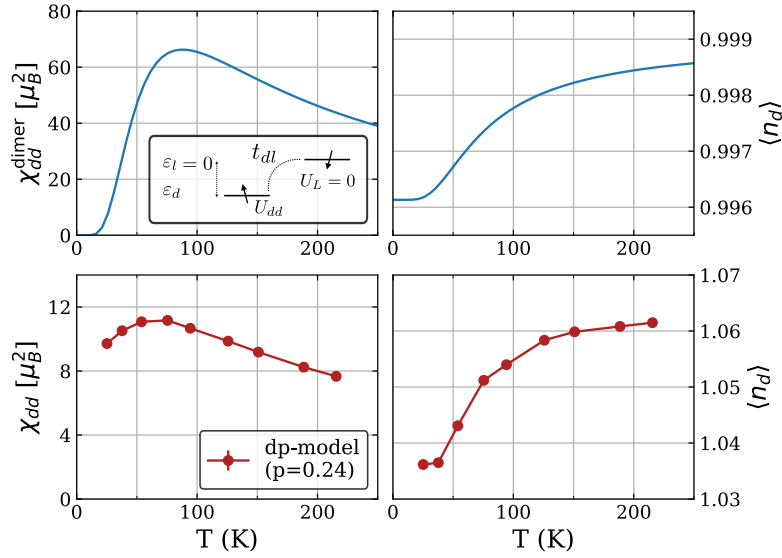


Figure 6: Insights into the DMFT data in the high doping limit $p = 0.24$ (lower panels) from the asymmetric dimer model (upper panels): Magnetic susceptibility χ_{dd} and density n_d show the same trend as a function of temperature in both models. The unscreened moment of the dimer leads to a susceptibility which is about one order of magnitude larger than in DMFT.

B The asymmetric dimer model

In order to aid with the interpretation of our main results for the temperature and doping dependence of the magnetic susceptibility and orbital occupation in the Emery model calculated with single-site DMFT, we consider a minimal toy model by replacing the bath with a single ligand, which can reproduce the simultaneous changes of d-occupation and susceptibility with temperature. The small cluster as a minimal toy model can be “derived” from a single isolated unit-cell of the Emery model. Within the unit-cell we can rotate the oxygen basis to a bonding and a (fully occupied and decoupled) non-bonding ligand state. The bonding ligand together with Cu $d_{x^2-y^2}$ forms an *asymmetric* Hubbard dimer which we can solve analytically (the results for ground and first excited state can be found in Tab. 1).

The Hamiltonian reads

$$\hat{H} = \sum_{\sigma} (\varepsilon_l \hat{n}_{l,\sigma} + t_{dl} (\hat{c}_{d\sigma}^{\dagger} \hat{c}_{l\sigma} + \hat{c}_{l\sigma}^{\dagger} \hat{c}_{d\sigma})) + U_{dd} \hat{n}_{d\uparrow} \hat{n}_{d\downarrow}, \quad (10)$$

with $t_{dl} = 1.93$ eV, $\varepsilon_l - \varepsilon_d = 2.15$ eV and the onsite interaction of the $d_{x^2-y^2}$ orbital $U_{dd} = 9.1$ eV. To approach the doped cases, we analyze the dimer at half-filling which corresponds to a filling of $N = 4$ in the Emery model and, therefore, represents the high doping limit. In Fig. 6 we show the resulting plots of the susceptibility together with temperature-dependent occupations of the $d_{x^2-y^2}$ orbital in the dimer-model as well as the corresponding DMFT plots at the highest considered doping level.

Due to the limitations of our toy model, which completely neglects finite bandwidth effects and is fixed to the high doping limit, we cannot compare the plots on a quantitative scale. While we refrain from over-complicating the toy model by fitting its parameters to the DMFT result, we fix the d-orbital parameter but rescale the ligand parameter $t_{dl} = 0.1$ eV to fit the effect of the hybridization function and to obtain a temperature

Table 1: Eigenvalues and eigenvectors of the ground state and first excited state, respectively, of an asymmetric dimer. The notation $|\downarrow, \uparrow\rangle$ indicates spin down on d-site and spin up on ligand. The singlet state is the ground state, which causes decreasing susceptibility at lower temperatures.

energy (eV)	eigenvector
0	$0.7 \uparrow, \downarrow\rangle - 0.7 \downarrow, \uparrow\rangle + 0.02 \uparrow\downarrow, 0\rangle + 0.07 0, \uparrow\downarrow\rangle$
≈ 0.02	$1/\sqrt{2}(\uparrow, \downarrow\rangle + \downarrow, \uparrow\rangle), \uparrow, \uparrow\rangle, \downarrow, \downarrow\rangle$

scale that coincides with the material realistic DMFT calculation. The data shown in Fig. 6 shows a qualitative agreement between the behavior of DMFT and the asymmetric dimer model for both the $d_{x^2-y^2}$ occupation and downturn of the uniform susceptibility (It should be noted that due to the much reduced screening of the impurity moment, the susceptibility in the dimer is about ten times larger than the DMFT result).

The downturn of χ_{dd} at low-temperature regions in the dimer model can be traced back to the increased dominance of its singlet ground state (i.e., the local limit of the Zhang-Rice singlet). Importantly, the asymmetry of the dimer between copper $3d$ orbital and oxygen $2p$ ligand leads to a non-negligible temperature-dependent change of the $d_{x^2-y^2}$ occupation. Such a change would be completely absent in a symmetric dimer model which would be the corresponding toy-model for the single-band Hubbard model.

References

- [1] J. G. Bednorz and K. A. Müller, *Possible high T_c superconductivity in the Ba-La-Cu-O system*, *Zeitschrift für Physik B Condensed Matter* **64**, 189 (1986), doi:10.1007/BF01303701.
- [2] B. Keimer, S. A. Kivelson, M. R. Norman, S. Uchida and J. Zaanen, *From quantum matter to high-temperature superconductivity in copper oxides*, *Nature* **518**(7538), 179 (2015), doi:10.1038/nature14165.
- [3] J. Hubbard, *Electron Correlations in Narrow Energy Bands*, *Proceedings of the Royal Society of London. Series A, Mathematical and Physical Sciences* **276**, 238 (1963), doi:10.1098/rspa.1963.0204.
- [4] J. Hubbard and B. H. Flowers, *Electron correlations in narrow energy bands iii. an improved solution*, *Proc. R. Soc. London, Sect. A* **281**, 401 (1964), doi:10.1098/rspa.1964.0190.
- [5] M. C. Gutzwiller, *Effect of Correlation on the Ferromagnetism of Transition Metals*, *Phys. Rev. Lett.* **10**, 159 (1963), doi:10.1103/PhysRevLett.10.159.
- [6] J. Kanamori, *Electron Correlation and Ferromagnetism of Transition Metals*, *Prog. Theor. Phys.* **30**, 275 (1963), doi:10.1143/PTP.30.275.
- [7] V. J. Emery, *Theory of high- t_c superconductivity in oxides*, *Phys. Rev. Lett.* **58**, 2794 (1987), doi:10.1103/PhysRevLett.58.2794.
- [8] O. Andersen, A. Liechtenstein, O. Jepsen and F. Paulsen, *Lda energy bands, low-energy hamiltonians, $t', t'', t_{\text{perp}}(k)$, and j_{perp}* , *Journal of Physics and Chemistry of Solids* **56** (1995), doi:10.1016/0022-3697(95)00269-3.

- [9] M. Qin, T. Schäfer, S. Andergassen, P. Corboz and E. Gull, *The Hubbard Model: A Computational Perspective*, Annual Review of Condensed Matter Physics **13** (2022), doi:10.1146/annurev-conmatphys-090921-033948.
- [10] D. P. Arovas, E. Berg, S. A. Kivelson and S. Raghu, *The Hubbard Model*, Annual Review of Condensed Matter Physics **13** (2022), doi:10.1146/annurev-conmatphys-031620-102024.
- [11] P. A. Lee, N. Nagaosa and X.-G. Wen, *Doping a Mott insulator: Physics of high-temperature superconductivity*, Rev. Mod. Phys. **78**, 17 (2006), doi:10.1103/RevModPhys.78.17.
- [12] N. P. Armitage, P. Fournier and R. L. Greene, *Progress and perspectives on electron-doped cuprates*, Rev. Mod. Phys. **82**, 2421 (2010), doi:10.1103/RevModPhys.82.2421.
- [13] W. Metzner and D. Vollhardt, *Correlated Lattice Fermions in $d = \infty$ Dimensions*, Phys. Rev. Lett. **62**, 324 (1989), doi:10.1103/PhysRevLett.62.324.
- [14] A. Georges and G. Kotliar, *Hubbard model in infinite dimensions*, Phys. Rev. B **45**, 6479 (1992), doi:10.1103/PhysRevB.45.6479.
- [15] A. Georges, G. Kotliar, W. Krauth and M. J. Rozenberg, *Dynamical mean-field theory of strongly correlated fermion systems and the limit of infinite dimensions*, Rev. Mod. Phys. **68**, 13 (1996), doi:10.1103/RevModPhys.68.13.
- [16] H. Alloul, T. Ohno and P. Mendels, *^{89}Y nmr evidence for a fermi-liquid behavior in $\text{YBa}_2\text{Cu}_3\text{O}_{6+x}$* , Phys. Rev. Lett. **63**, 1700 (1989), doi:10.1103/PhysRevLett.63.1700.
- [17] T. Timusk and B. Statt, *The pseudogap in high-temperature superconductors: an experimental survey*, Reports on Progress in Physics **62**(1), 61 (1999), doi:10.1088/0034-4885/62/1/002.
- [18] M. V. Sadovskii, *Pseudogap in high-temperature superconductors*, Physics-Usppekhi **44**(5), 515 (2001), doi:10.1070/PU2001v044n05ABEH000902.
- [19] A. V. Puchkov, D. N. Basov and T. Timusk, *The pseudogap state in high- superconductors: an infrared study*, Journal of Physics: Condensed Matter **8**(48), 10049 (1996), doi:10.1088/0953-8984/8/48/023.
- [20] M. Takigawa, A. P. Reyes, P. C. Hammel, J. D. Thompson, R. H. Heffner, Z. Fisk and K. C. Ott, *Cu and O NMR studies of the magnetic properties of $\text{YBa}_2\text{Cu}_3\text{O}_{6.63}$ ($T_c=62\text{ K}$)*, Phys. Rev. B **43**, 247 (1991), doi:10.1103/PhysRevB.43.247.
- [21] S. Ohsugi, Y. Kitaoka, K. Ishida, G.-q. Zheng and K. Asayama, *Cu NMR and NQR Studies of High- T_c Superconductor $\text{La}_{2-x}\text{Sr}_x\text{CuO}_4$* , Journal of the Physical Society of Japan **63**(2), 700 (1994), doi:10.1143/JPSJ.63.700.
- [22] S. Ohsugi, Y. Kitaoka and K. Asayama, *Temperature dependence of spin susceptibility of $\text{La}_{2-x}\text{Sr}_x\text{CuO}_4$ knight shift measurement*, Physica C: Superconductivity **282-287**, 1373 (1997), doi:https://doi.org/10.1016/S0921-4534(97)00773-9, Proceedings of the International Conference on Materials and Mechanisms of Superconductivity High Temperature Superconductors V.
- [23] T. Maier, M. Jarrell, T. Pruschke and M. H. Hettler, *Quantum cluster theories*, Rev. Mod. Phys. **77**, 1027 (2005), doi:10.1103/RevModPhys.77.1027.

- [24] G. Rohringer, H. Hafermann, A. Toschi, A. A. Katanin, A. E. Antipov, M. I. Katsnelson, A. I. Lichtenstein, A. N. Rubtsov and K. Held, *Diagrammatic routes to nonlocal correlations beyond dynamical mean field theory*, Rev. Mod. Phys. **90**, 025003 (2018), doi:10.1103/RevModPhys.90.025003.
- [25] P. Hansmann, X. Yang, A. Toschi, G. Khaliullin, O. K. Andersen and K. Held, *Turning a nickelate fermi surface into a cupratelike one through heterostructuring*, Phys. Rev. Lett. **103**, 016401 (2009), doi:10.1103/PhysRevLett.103.016401.
- [26] P. Hansmann, A. Toschi, X. Yang, O. K. Andersen and K. Held, *Electronic structure of nickelates: From two-dimensional heterostructures to three-dimensional bulk materials*, Phys. Rev. B **82**, 235123 (2010), doi:10.1103/PhysRevB.82.235123.
- [27] A. Tamai, M. Zingl, E. Rozbicki, E. Cappelli, S. Ricc3, A. de la Torre, S. M. Walker, F. Y. Bruno, P. D. C. King, W. Meevasana, M. Shi, M. Radovi3 *et al.*, *High-resolution photoemission on sr2ruo4 reveals correlation-enhanced effective spin-orbit coupling and dominantly local self-energies*, Physical Review X (2018).
- [28] S. K3ser, H. U. R. Strand, N. Wentzell, A. Georges, O. Parcollet and P. Hansmann, *Interorbital singlet pairing in sr2ruo4: A hund's superconductor*, Phys. Rev. B **105**, 155101 (2022), doi:10.1103/PhysRevB.105.155101.
- [29] M. B. Z3lfl, T. Maier, T. Pruschke and J. Keller, *Electronic properties of cuo2-planes: A dmft study*, The European Physical Journal B - Condensed Matter and Complex Systems **13**(1), 47 (2000).
- [30] C. Weber, K. Haule and G. Kotliar, *Optical weights and waterfalls in doped charge-transfer insulators: A local density approximation and dynamical mean-field theory study of la2-xsr_xcuo4*, Phys. Rev. B **78**, 134519 (2008), doi:10.1103/PhysRevB.78.134519.
- [31] L. de' Medici, X. Wang, M. Capone and A. J. Millis, *Correlation strength, gaps, and particle-hole asymmetry in high-Tc cuprates: A dynamical mean field study of the three-band copper-oxide model*, Phys. Rev. B **80**, 054501 (2009), doi:10.1103/PhysRevB.80.054501.
- [32] P. Hansmann, N. Parragh, A. Toschi, G. Sangiovanni and K. Held, *Importance of d-p coulomb interaction for high tc cuprates and other oxides*, New Journal of Physics **16**(3), 033009 (2014), doi:10.1088/1367-2630/16/3/033009.
- [33] M. Avramovska, D. Pavi3evi3 and J. Haase, *Nmr shift and relaxation and the electronic spin of superconducting cuprates*, Journal of Superconductivity and Novel Magnetism **33**(9), 2621 (2020), doi:10.1007/s10948-020-05498-y.
- [34] C. Weber, C. Yee, K. Haule and G. Kotliar, *Scaling of the transition temperature of hole-doped cuprate superconductors with the charge-transfer energy*, Europhysics Letters **100**(3), 37001 (2012), doi:10.1209/0295-5075/100/37001.
- [35] N. Kowalski, S. S. Dash, P. S3mon, D. S3n3chal and A.-M. Tremblay, *Oxygen hole content, charge-transfer gap, covalency, and cuprate superconductivity*, Proceedings of the National Academy of Sciences **118**(40), e2106476118 (2021), doi:10.1073/pnas.2106476118.
- [36] E. Gull, A. J. Millis, A. I. Lichtenstein, A. N. Rubtsov, M. Troyer and P. Werner, *Continuous-time Monte Carlo methods for quantum impurity models*, Rev. Mod. Phys. **83**, 349 (2011), doi:10.1103/RevModPhys.83.349.

- [37] M. Wallerberger, A. Hausoel, P. Gunacker, A. Kowalski, N. Parragh, F. Goth, K. Held and G. Sangiovanni, *w2dynamics: Local one- and two-particle quantities from dynamical mean field theory*, Computer Physics Communications **235**, 388 (2019), doi:<https://doi.org/10.1016/j.cpc.2018.09.007>.
- [38] D. Bergeron and A.-M. S. Tremblay, *Algorithms for optimized maximum entropy and diagnostic tools for analytic continuation*, Phys. Rev. E **94**, 023303 (2016), doi:[10.1103/PhysRevE.94.023303](https://doi.org/10.1103/PhysRevE.94.023303).
- [39] F. C. Zhang and T. M. Rice, *Effective hamiltonian for the superconducting cu oxides*, Phys. Rev. B **37**, 3759 (1988), doi:[10.1103/PhysRevB.37.3759](https://doi.org/10.1103/PhysRevB.37.3759).
- [40] S. Uchida, T. Ido, H. Takagi, T. Arima, Y. Tokura and S. Tajima, *Optical spectra of $\text{La}_{2-x}\text{Sr}_x\text{CuO}_4$: Effect of carrier doping on the electronic structure of the CuO_2 plane*, Phys. Rev. B **43**, 7942 (1991), doi:[10.1103/PhysRevB.43.7942](https://doi.org/10.1103/PhysRevB.43.7942).
- [41] T. Yoshida, X. J. Zhou, K. Tanaka, W. L. Yang, Z. Hussain, Z.-X. Shen, A. Fujimori, S. Sahrakorpi, M. Lindroos, R. S. Markiewicz, A. Bansil, S. Komiyama *et al.*, *Systematic doping evolution of the underlying fermi surface of $\text{La}_{2-x}\text{Sr}_x\text{CuO}_4$* , Phys. Rev. B **74**, 224510 (2006), doi:[10.1103/PhysRevB.74.224510](https://doi.org/10.1103/PhysRevB.74.224510).
- [42] V. Barzykin and D. Pines, *Magnetic scaling in cuprate superconductors*, Phys. Rev. B **52**, 13585 (1995), doi:[10.1103/PhysRevB.52.13585](https://doi.org/10.1103/PhysRevB.52.13585).
- [43] K. Ishida, K. Yoshida, T. Mito, Y. Tokunaga, Y. Kitaoka, K. Asayama, Y. Nakayama, J. Shimoyama and K. Kishio, *Pseudogap behavior in single-crystal $\text{Bi}_2\text{Sr}_2\text{CaCu}_2\text{O}_{8+\delta}$ probed by cu nmr*, Phys. Rev. B **58**, R5960 (1998), doi:[10.1103/PhysRevB.58.R5960](https://doi.org/10.1103/PhysRevB.58.R5960).
- [44] X. Chen, J. P. F. Leblanc and E. Gull, *Simulation of the NMR response in the pseudogap regime of the cuprates*, Nature Communications **8**, 14986 (2017), doi:[10.1038/ncomms14986](https://doi.org/10.1038/ncomms14986).
- [45] M. Klett, P. Hansmann and T. Schäfer, *Magnetic Properties and Pseudogap Formation in Infinite-Layer Nickelates: Insights From the Single-Band Hubbard Model*, Frontiers in Physics **10** (2022), doi:[10.3389/fphy.2022.834682](https://doi.org/10.3389/fphy.2022.834682).
- [46] M. Kitatani, L. Si, O. Janson, R. Arita, Z. Zhong and K. Held, *Nickelate superconductors—a renaissance of the one-band Hubbard model*, npj Quantum Materials **5**(1) (2020), doi:[10.1038/s41535-020-00260-y](https://doi.org/10.1038/s41535-020-00260-y).
- [47] R. A. Ortiz, H. Menke, F. Misják, D. T. Mantadakis, K. Fürsich, E. Schierle, G. Logvenov, U. Kaiser, B. Keimer, P. Hansmann and E. Benckiser, *Superlattice approach to doping infinite-layer nickelates*, Phys. Rev. B **104**, 165137 (2021), doi:[10.1103/PhysRevB.104.165137](https://doi.org/10.1103/PhysRevB.104.165137).
- [48] R. A. Ortiz, P. Puphal, M. Klett, F. Hotz, R. K. Kremer, H. Trepka, M. Hemmida, H.-A. K. von Nidda, M. Isobe, R. Khasanov, H. Luetkens, P. Hansmann *et al.*, *Magnetic correlations in infinite-layer nickelates: An experimental and theoretical multimethod study*, Phys. Rev. Res. **4**, 023093 (2022), doi:[10.1103/PhysRevResearch.4.023093](https://doi.org/10.1103/PhysRevResearch.4.023093).